Experimental and theoretical investigation of the excitation of discharge pressure pulsations by a screw compressor with variable inner volume ratio

A. Linkamp, **A. Brümmer**
Chair of Fluidics, TU Dortmund University, Dortmund

Abstract

In the present paper the influence of a screw compressor's outlet geometry on discharge pressure pulsations is experimentally investigated and compared to theory. Pressure pulsations in the discharge piping of a screw compressor with variable inner volume ratio provided by switchable additional outlet ducts in the casing are measured for different discharge pressures and rotational speeds. Thereby the potential to reduce pulsations by adapting the compressor's inner volume ratio v_i to the outer (system) pressure ratio by means of the concept of pre-outlet ducts is determined. The experimental results are further analysed by separating the transient pressure signals into incident and reflected waves in the frequency domain in order to obtain the compressor's pulsation excitation. Additionally the excitation of discharge pressure pulsations is calculated using a theoretical, one-dimensional approach and compared to the experimental results.

Notation

A	[m²]	area	a	[m/s]	speed of sound
$\underline{A}/\underline{B}$	[-]	complex amplitude	c	[m/s]	flow velocity
c_v	[J/kg K]	isochoric heat capacity	f_x	[m/s^2]	specific frictional force
f_{pp}	[Hz]	pocket pass frequency	I	[W/m²]	intensity
j	[-]	imaginary unit	k	[1/m]	wave number
L_W	[dB]	sound power level	L_p	[dB]	sound pressure level
n	[rpm]	rotational speed	P	[W]	power
p	[bar]	Pressure	R	[J/kg K]	specific gas constant
T	[K]	temperature	u	[J/kg]	specific internal energy
V	[m²]	volume	v_i	[-]	inner volume ratio
w	[J/kg]	specific work	x	[m]	spatial distance
η	[-]	efficiency	π	[-]	pressure ratio
ρ	[kg/m^3]	density	ω	[rad/s]	angular velocity

1 Introduction

Pressure pulsation excitation is an important criterion when evaluating the operating behaviour of screw compressors. High pressure pulsations not only indicate power dissipation, but are also a main cause of noise and vibration in an attached system [1]. Besides geometrical parameters, operational parameters such as the difference between chamber pressure and discharge pressure significantly influence discharge pressure pulsation excitation [2,3]. In case of varying outer pressure ratio π_o, adapting the inner volume ratio v_i of a screw compressor is thus a key factor for reducing pulsation excitation. Especially in refrigeration applications this adaption is often realised by means of a slide valve [4,5]. Due primarily to frictional problems this approach is not suitable for dry-running screw compressors. In the present work the potential to reduce pulsation excitation by means of pre-outlets is investigated theoretically and experimentally. The focus is on a fairly simple constructive realisation of the adaption of the inner volume ratio.

The theoretical approach is based on the author's previous work [6]. The screw compressor is modelled one-dimensionally using the method of characteristics. The method of characteristics is a technique to transform a system of partial differential equations into ordinary differential equations. Applied to a system of conservation laws the resulting set of linear equations is solved exactly, thus no iterative errors occur. The method of characteristics is widely used for calculating transient flow in piping systems attached to displacement machines [6,7,8]. The model's main emphasis is a one-dimensional adaptive grid of the working chamber as well as the method for calculating the transient, compressible and dissipative flow through the outlet port with time-dependent area in order to obtain as accurate a prediction as possible regarding the excitation of pressure and flow pulsations by screw compressors, while keeping the modelling effort and computational effort within reasonable limits. This model is applied to the investigated screw compressor with multiple outlet areas.

2 Theoretical background

2.1 One-dimensional calculation of pulsating flow

The calculations are carried out using a transient, compressible solver based on the method of characteristics, in particular using two characteristics. These two characteristics are derived from the conservation of mass and the conservation of momentum. The system is extended by a transient form of the conservation of energy to model convective transport of energy.

The governing equations are applied in differential form. The one-dimensional, transient form of the conservation of mass reads

$$\frac{\partial \rho}{\partial t} + c \cdot \frac{\partial \rho}{\partial x} + \rho \cdot \frac{\partial c}{\partial x} = 0\,. \tag{1}$$

The conservation of momentum in the compressible, one-dimensional, transient case results in

$$\frac{\partial c}{\partial t} + c \cdot \frac{\partial c}{\partial x} + \frac{1}{\rho} \cdot \frac{\partial p}{\partial x} + f_x = 0. \tag{2}$$

As is common for gas flows, the influence of gravity is neglected in equation (2). The specific force term f_x represents pipe wall friction. The conservation of energy for an adiabatic system and an ideal gas with $du = c_v\, dT$ reads

$$\frac{\partial T}{\partial t} + c \cdot \frac{\partial T}{\partial x} + \frac{RT}{c_v} \cdot \frac{\partial c}{\partial x} = 0. \tag{3}$$

To close the system for the four flow variables p, c, ρ, T the equation of state is used, which for an ideal gas generally reads

$$p = \rho \cdot R \cdot T. \tag{4}$$

These two characteristic equations are derived from the conservations of mass and momentum, respectively. Therefore a change of variables is necessary to reduce the number of variables in this subsystem of two equations. The primitive variables p and c are chosen in order to easily apply boundary conditions given directly by these variables. The partial differential equation system for the state variables p and c can then be transformed into a system of ordinary differential equations, which reads [6]

$$\frac{dp}{dt} + \rho \cdot a \cdot \frac{dc}{dt} + \rho \cdot a \cdot f_x = 0 \qquad \text{for} \qquad \frac{dx}{dt} = c + a \tag{5}$$

$$\frac{dp}{dt} - \rho \cdot a \cdot \frac{dc}{dt} - \rho \cdot a \cdot f_x = 0 \qquad \text{for} \qquad \frac{dx}{dt} = c - a. \tag{6}$$

The ordinary differential equation system (5-6) is henceforth only valid along the characteristic directions of the derivations. These are referred to as characteristics and read, for the one-dimensional flow problem dealt with here,

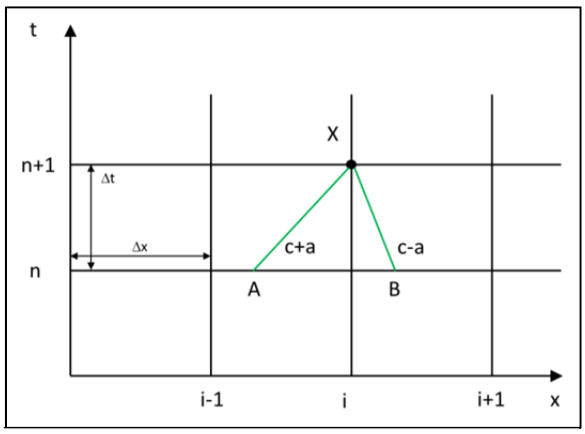

Fig. 1: Time-space-grid

$$\frac{dx}{dt} = c + a \tag{7}$$

$$\frac{dx}{dt} = c - a \tag{8}$$

The physical significance of the characteristics lies in the propagation of information, i.e. of small changes in the gas state, in the one-dimensional flow domain. Information propagation takes place along the

characteristics at the speed (c+a) in the downstream direction and at the speed (a-c) in the upstream direction.

For a numerical solution the differential equations are transformed into difference equations. The characteristic equations are linearised assuming a sufficiently fine spatial and temporal discretisation. The gradients of the characteristics (Eq. (5) and (6)) are thus regarded as constant. Furthermore, the characteristic acoustic impedance is assumed to be constant through a computational step. For calculation, the one-dimensional discretisation of the physical domain leads to a two-dimensional time-space-grid as can be seen in **Fig. 1**. The calculation of pressure p and velocity c at the current grid point X at space step i and time step n+1 is based on the known values at time step n, whereby the unknown values at the base points A and B are linearly interpolated between the known values in the adjacent grid points. The discretisation results in the following characteristic equations:

$$\frac{\Delta p}{\Delta t} + \rho \cdot a \cdot \frac{\Delta c}{\Delta t} + \rho \cdot a \cdot f_x = 0 \qquad \text{for} \qquad \frac{\Delta x}{\Delta t} = c + a \tag{9}$$

$$\frac{\Delta p}{\Delta t} - \rho \cdot a \cdot \frac{\Delta c}{\Delta t} - \rho \cdot a \cdot f_x = 0 \qquad \text{for} \qquad \frac{\Delta x}{\Delta t} = c - a \tag{10}$$

with the increments for variables p and c given by the gradients of the characteristics:

$$\frac{\Delta p}{\Delta t} = \frac{p_X - p_A}{\Delta t} \tag{11}$$

$$\frac{\Delta c}{\Delta t} = \frac{c_X - c_A}{\Delta t}. \tag{12}$$

In order to calculate temperature T, the energy equation is also linearised. For this purpose the differentials are in turn transformed into quotients of finite differences. Based on the space-time grid (Fig. 1), the following results for a positive direction of flow:

$$\frac{\partial T}{\partial t} \approx \frac{\Delta T}{\Delta t} = \frac{T_i^{n+1} - T_i^n}{\Delta t} \tag{13}$$

$$\frac{\partial T}{\partial x} \approx \frac{\Delta T}{\Delta x} = \frac{T_i^n - T_{i-1}^n}{\Delta \mathrm{x}}. \tag{14}$$

With equations (13-14), the following linear relationship follows from equation (3) for the temperatures in the space-time grid as a function of positive flow velocity c.

$$\frac{T_i^{n+1} - T_i^n}{\Delta t} + c_i^n \cdot \frac{T_i^n - T_{i-1}^n}{\Delta x} + \frac{R \cdot T_i^n}{c_v} \cdot \frac{c_i^n - c_{i-1}^n}{\Delta x} = 0 \tag{15}$$

Subsequently, density ρ can be determined via the equation of state (4), meaning the state at point X at time (n+1) is fully known. For a more detailed derivation, see the author's previous work [6].

2.2 Modelling of a screw compressor with pre-outlets

Due to the one-dimensionality, the working chamber is modelled as a cylindrical element with constant diameter and variable length. The initial length of the working chamber l_0 is

determined in accordance with the difference between the crown and root circle diameter, $d_{c,m}$ and $d_{r,m}$ respectively, of the male rotor.

The time-dependent length of the working chamber $l_{wc}(t)$ results from the quotient of current volume $V_{wc}(t)$ and the constant area A_{wc}. The working chamber is re-discretised for each time step (adaptive grid) and the state variables are then converted from the old grid to the new grid. The flow velocity $c_{wc}(t)$ determined from the derivation of the volume curve $V_{wc}(t)$ and the constant working chamber area A_{wc} is defined as a boundary condition on the "left side" of the segment, cf. [6].

The flow through the main outlet area as well as the pre-outlets is modelled as an orifice flow through a circular orifice. Thereby the focus is placed on the determination of critical flow in the narrowest diameter, which is an important effect in the discharge process of screw compressors, cf. [6]. Due to multiple existing outlet areas, the working chamber is connected to several orifices. This leads to the structure of the compressor model shown in **Fig. 2**.

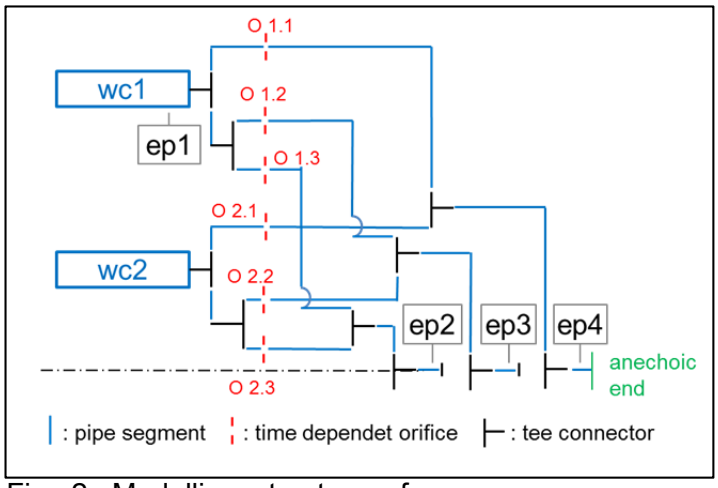

Fig. 2: Modelling structure of a screw compressor with multiple outlet areas

For simplicity, half of the model, which is symmetric to the dotted line, is shown. Since four working chambers of the investigated compressor are in operation (compressing or discharging) simultaneously, the model consists of four working chambers. As can be seen in Fig. 2 each working chamber (wc) is connected to three independent orifices (e.g. O 1.1).

All model elements on the left side of these orifices are part of the working chamber. All elements on the right side of the orifices represent the compressor's discharge domain, including the pre-outlet ducts. The first pipe segments connected to the pre-outlets (O X.2, O X.3) on the high pressure side represent the pre-outlet ducts, which are bores in the compressor casing (cf. chap. 3). Thus the influence of the geometry of the pre-outlet ducts is considered in the presented model. Evaluation points (ep1-4) for the following evaluation of the pressure development (cf. chap.4) are also indicated.

The boundary condition at the downstream end of the computational domain is anechoic. Thus, the pure pulsation excitation of a screw compressor is calculated independent of a piping system. The application of one-dimensional approaches and theories implies that

solely plane waves are calculated. Multidimensional effects such as cross-wall modes cannot be taken into account.

In the presented model all clearance flows are ignored. This means that solely the flow through the main outlet and the pre-outlets is calculated. The chamber filling process is also not simulated. The working chamber is always initialized in closed state at maximum chamber volume. The gas state at the time of initialization corresponds to the assumed suction-side state. This approach is consistent with the assumption of a complete and non-throttled chamber filling.

3 Investigated screw compressor

The machine examined is a screw compressor with four lobes on the male rotor and six lobes on the female rotor. The original inner volume ratio amounts to $v_i = 2.0$. The variable inner volume ratio is realized by bores (pre-outlet ducts) in the compressor casing, which lead from the working chamber to the discharge domain (**Fig. 3**). These bores are positioned in such a way that the inner volume ratio can be set from $v_i = 2.0$ to $v_i = 1.8$ or $v_i = 1.6$. Each of the two pre-outlet stages consist of a series of eight pre-outlet ducts with a diameter of 10 mm for the first stage ($v_i = 1.8$, in the following po1) and 12 mm for the second stage ($v_i = 1.6$, in the following po2).

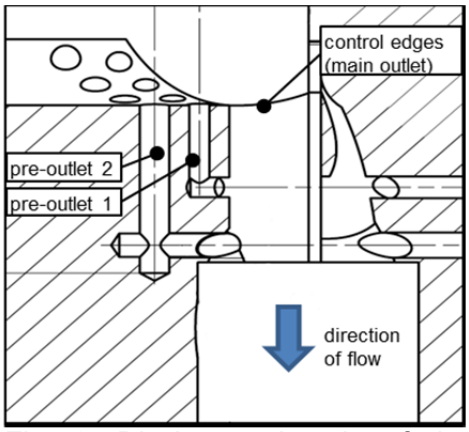

Fig. 3: Discharge domain of the investigated screw compressor with variable inner volume ratio

The inner volume ratio for these tests is adjusted by closing the pre-outlet ducts from their discharge domain end (horizontal bores in fig. 3). Since these ducts are connected to the working chamber even in a closed state, they act as dead spaces.

The normalized volume curve of the investigated compressor and the

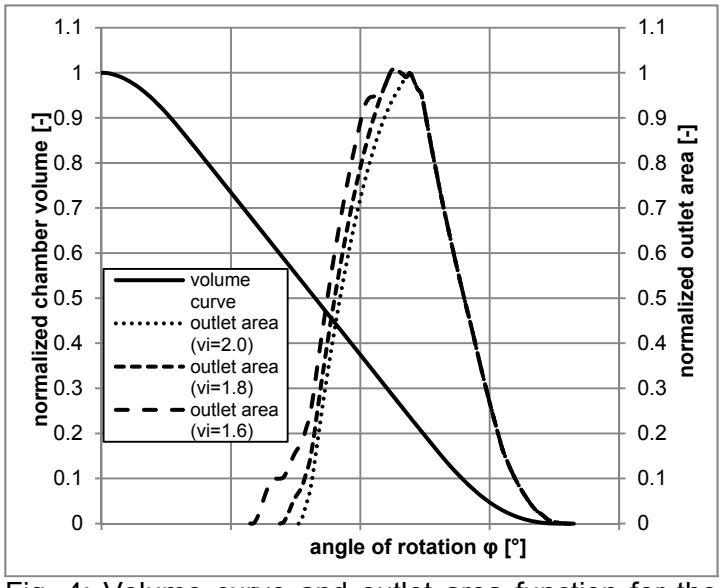

Fig. 4: Volume curve and outlet area function for the three inner volume ratios

normalized integral outlet area curves for the three adjustable inner volume ratios are shown in **Fig. 4**. The volume curve is related to maximum chamber volume and the outlet area functions are related to the maximum outlet area of the original casing with $v_i = 2.0$.

4 Simulation results

A series of simulations is carried out with different discharge pressures and rotational speeds. Initially pressure curves inside a working chamber are analysed; afterwards the resulting pulsation excitation is compared to experimental results.

4.1 Dynamic pressure curves inside the working chamber

Fig. 5 shows the pressure curves at the four evaluation points ep1-4 (cf. Fig.2) for the inner volume ratio of $v_i = 2.0$, which correspond to a theoretical inner pressure ratio of $\pi_{i,th} = 2.64$ (air: $\kappa = 1.4$). In this configuration the pre-outlet ducts act as dead spaces. The thick solid line represents the pressure inside the working chamber, whereas the thin solid line represents the pressure in the discharge domain. The dashed and dotted lines show the pressure curves in po1 and po2, respectively. The pressure curves for the discharge domain and the pre-outlet ducts show periodic behavior with the pocket-pass-frequency of $f_{pp} = 600$ Hz. That occurs because the pre-outlet ducts are connected to each of the parallel operating working chambers.

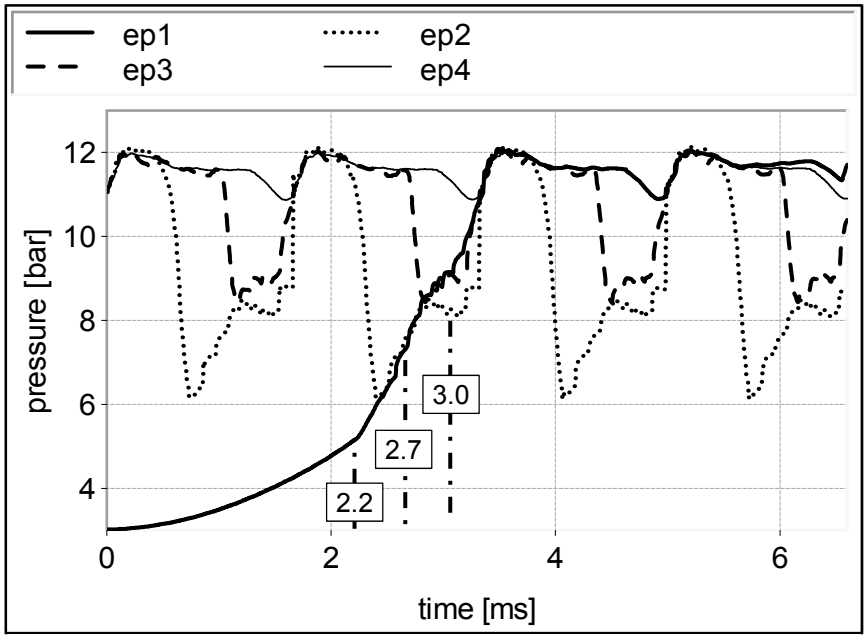

Fig. 5: Simulated pressure curves in the working chamber (ep1), po2 (ep2), po1 (ep3) and the discharge domain (ep4) for an inner volume ratio of $v_i = 2.0$, a rotational speed of n = 9000 rpm, a suction pressure of $p_s = 3$ bar and a discharge pressure of $p_d = 11.5$ bar

The pressure curve inside the working chamber shows a nearly isentropic compression up to 2.2 ms because clearance flows are neglected in the model; as a result, the only dissipative effect considered is wall friction, which is negligible due to the chosen geometry (large diameter, relatively short length). At 2.2 ms the working chamber is connected to po2, indicated by a pressure drop in the pre-outlet duct as well as an

accelerated pressure increase in the working chamber. At this point the pressure in po2 is close to the discharge pressure, leading to an expansion in the pre-outlet ducts.

Subsequently, at about 2.7 ms the connection between the working chamber and po1 is established, which can be recognized by the pressure equalization between these two domains.

At about 3 ms the working chamber is connected to the discharge domain via the main outlet (mo), a pressure equalization takes place and the pressure in the working chamber and the discharge domain correspond to each other. It is shown that due to the dead spaces embodied by the pre-outlet ducts, which are temporarily connected to the working chamber but not to the discharge domain, the pressure in the working chamber approaches the discharge pressure prior to the opening of the main outlet.

This behavior is caused by the pressure equalization between the working chamber and the pre-outlet ducts and leads to a reduction in the pulsation excitation because the pressure difference between the working chamber and the discharge domain is reduced. Thus compared to an equivalent compressor without these dead spaces, the closed pre-outlet ducts positively influence pulsation excitation but increase the power consumption due to the earlier pressure rise.

4.2 Influence of the inner volume ratio

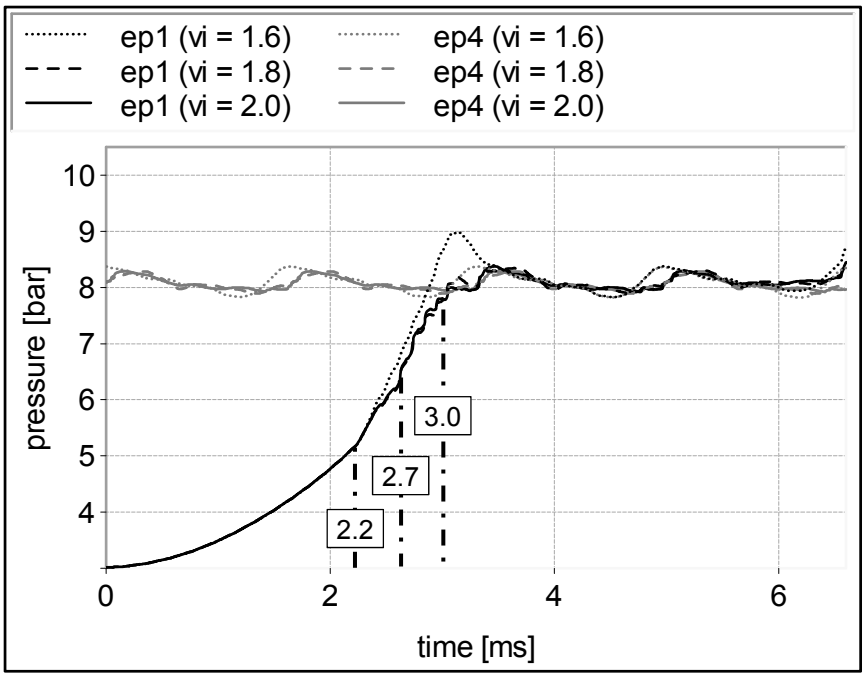

Fig. 6: Simulated pressure curves in the working chamber (ep1) and the discharge domain (ep4) for a rotational speed of n = 9000 rpm, a suction pressure of p_s = 3 bar and a discharge pressure of p_d = 8 bar

Fig. 6 shows simulated pressure curves in the working chamber and the discharge domain for the three inner volume ratios with a rotational speed of n = 9000 rpm, a suction pressure of p_s = 3 bar and a discharge pressure of p_d = 8 bar.

The connection to po2 is again established at 2.2 ms, whereby for the configuration where v_i = 1.6 a connection to the discharge domain is provided. For v_i = 1.8 and v_i = 2.0 respectively, the ducts are enclosed and thus act as dead

spaces. A change in the slope shortly after opening can be recognized in all three configurations, since a pressure equalization between the enclosed po2 ducts (finite volumes) and the working chamber takes place for $v_i = 1.8$ and $v_i = 2.0$. For $v_i = 1.6$, however, the pressure rises rapidly because the discharge side is regarded as an infinite volume with a constant discharge pressure.

The opening of po1 at 2.7 ms shows no significant influence on the pressure curve for $v_i = 1.6$. Furthermore, no significant difference between the pressure curves of the configuration with $v_i = 2.0$ and $v_i = 1.8$, now connected to the discharge side, can be recognized. When the main outlet opens at 3 ms, the pressure in the working chamber is close to the discharge pressure for both $v_i = 1.8$ and $v_i = 2.0$. For an inner volume ratio of $v_i = 1.6$, the pressure in the working chamber is slightly above the discharge pressure at this point in time and increases further, which indicates critical flow in the outlet area. This results in a pressure inside the working chamber that significantly exceeds the discharge pressure. A pressure equalization is reached at about 3.5 ms for this configuration.

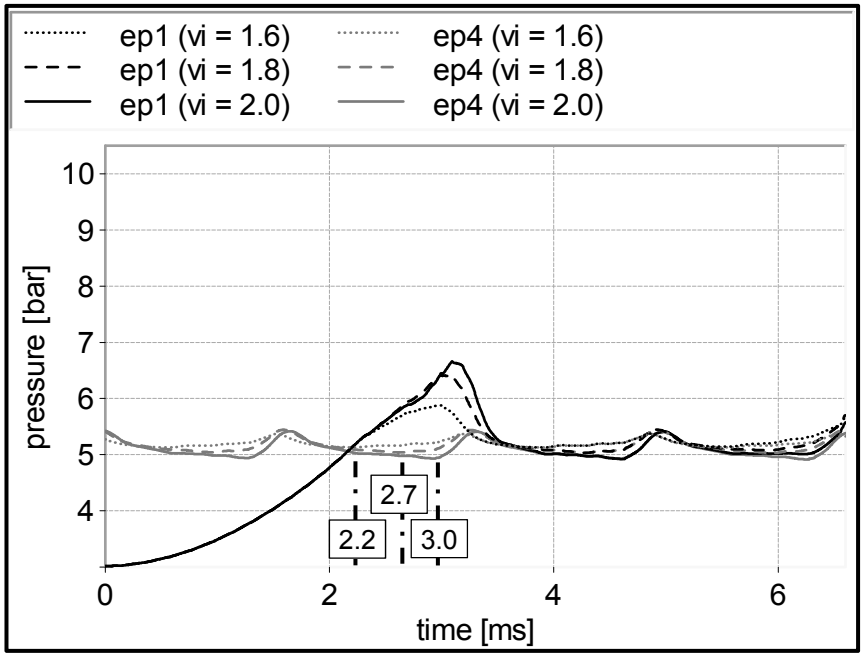

Fig. 7: Simulated pressure curves in the working chamber (ep1) and the discharge domain (ep4) for a rotational speed of n = 9000 rpm, a suction pressure of $p_s = 3$ bar and a discharge pressure of $p_d = 5.1$ bar

The respective pressure curves for a discharge pressure of $p_d = 5.1$ bar are shown in **Fig. 7**. In all three configurations an increasing overcome-pression takes place with also increasing inner volume ratio.

The effect of the pre-outlets can be clearly recognized in the pressure curves. The pressure gradient decreases shortly after the opening of po2 for $v_i = 1.6$. The maximum working chamber pressure increases with an increasing inner volume ratio, resulting in increasing discharge pressure pulsations as shown by the pressure curves in the discharge domain.

5 Experimental results

At first, the measured pressure pulsations are looked at in the form of sound pressure level L_p (reference: $2 \cdot 10^{-5}$ Pa effective in the frequency range of $f \leq 10$ kHz) of the pressure pulsations in the discharge piping. The evaluation of the potential to reduce pulsation excitation by means of the pressure signals measured in the discharge piping is based on the assumption, that a reduction in the excitation leads to a reduction in system response. Afterwards the experimental results are compared to simulation results by means of the sound power level L_W (reference: 10^{-12} W) of the pulsation excitation.

5.1 Experimental setup

For the experimental investigation of the adjustable compressor and the validation of the simulation results pulsation measurements were carried out. In order to compare the simulations and the experiments by means of pure excitation independent of the discharge piping, three axially offset piezo-electric relative pressure transducers ($mp_{1\text{-}3}$) were installed in the discharge housing and the discharge piping **(Fig. 8)**.

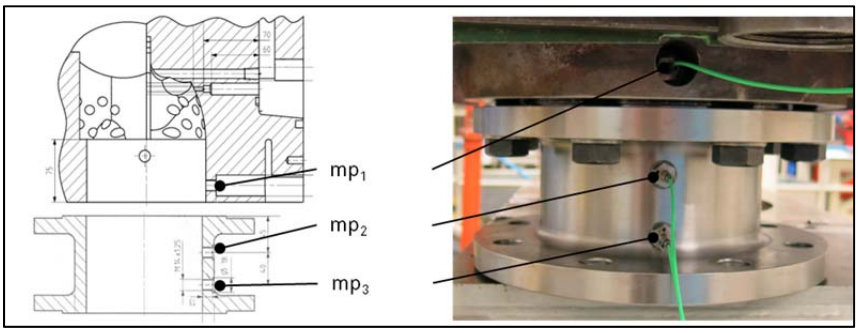

Fig. 8: positions of the piezo-electric pressure transducers in the discharge housing and the discharge piping

Furthermore the average pressure and temperature on the suction and discharge side of the compressor as well as the rotational speed were measured. The suction pressure is set to $p_s = 3$ bar during the measurements. For two different rotational speeds of $n = 9000$ rpm and $n = 12000$ rpm respectively, the discharge pressure p_d and thus the outer pressure ratio π_o is varied in the range of $1.4 \leq \pi_o \leq 2.7$.

5.2 Discharge pressure pulsations

The experimental results at an exemplary measuring point (mp_3) are looked at in the following. Qualitatively the values measured at the various measuring points correspond to each other. **Fig. 9** shows the sound pressure levels of the measured pressure pulsations inside the discharge piping for a suction pressure of $p_s = 3$ bar, a rotational speed of $n = 9000$ rpm and $n = 12000$ rpm, respectively, as well as the three adjustable inner volume ratios. The dashed lines indicate the theoretical inner pressure ratios $\pi_{i,th}$ (air: $\kappa = 1.4$) corresponding to the three inner volume ratios.

It can be clearly seen that the pressure pulsations are reduced by adapting the inner volume ratio to the outer pressure ratio for both n = 9000 rpm and n = 12000 rpm. For lower outer pressure ratios, the lowest pressure pulsations are measured with an inner volume ratio of v_i = 1.6. Equally, for high outer pressure ratios the lowest pressure pulsations are achieved with an inner volume ratio of v_i = 2.0.

The pressure pulsations measured generally increase along with rotational speed leading to a tendentially higher reduction by adapting the inner volume ratio. At the highest outer pressure ratio of π_o = 2.7 and a rotational speed of n = 9000 rpm, the sound pressure level is reduced by 2 dB by increasing the inner volume ratio from 1.8 to 2.0. The reduction amounts to 3 dB for a rotational speed of n = 12000 rpm.

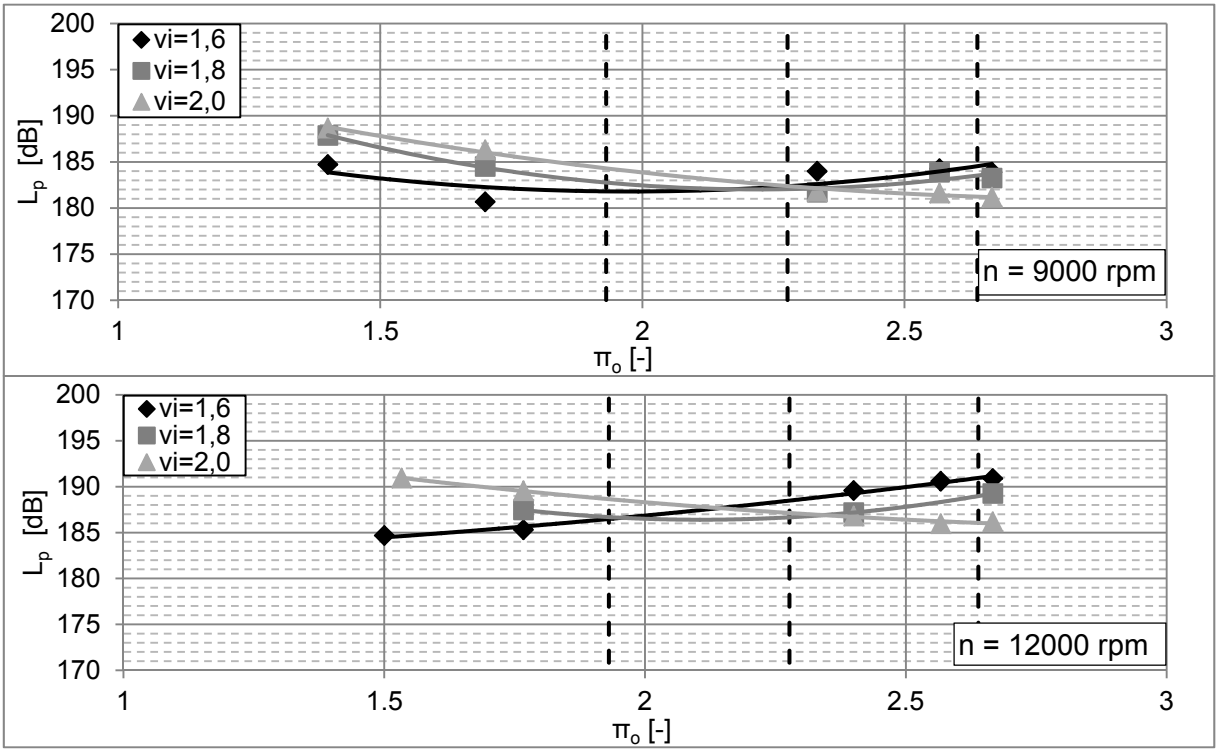

Fig. 9: Sound pressure level L_p of the measured pressure pulsations at mp3 for a suction pressure of p_s = 3 bar and a rotational speed of n = 9000 rpm and n = 12000 rpm for different inner volume ratios

5.3 Power consumption

Another effect of the adaption of the inner volume ratio is a decrease in power consumption due to a reduction of over- or undercompression. Power consumption of the screw compressor investigated is evaluated by means of polytropic, effective efficiency $\eta_{p,e}$. Therefore, the specific polytropic work $w_{f,p}$ is determined for each operating point based on a polytropic exponent calculated from the mean pressure and the temperature on the suction and discharge side. The specific polytropic work describes the usable work transferred to the

working fluid. The specific effective work w_e is obtained by means of measured effective Power P_e and mass flow ṁ. The polytropic, effective efficiency reads

$$\eta_{e,p} = \frac{w_{f,p}}{w_e}. \tag{16}$$

In **Fig. 10** the polytropic, effective efficiency for a suction pressure of p_s = 3 bar and a rotational speed of n = 9000 rpm and n = 12000 rpm is presented as a function of the outer pressure ratio. At a rotational speed of n = 9000 rpm, an increasing efficiency arises for a decreasing inner volume ratio v_i at low outer pressure ratios (e.g. π_o = 1.4). The lowest efficiency at high outer pressure ratios can be recognized for an inner volume ratio of v_i = 1.6. Between v_i = 1.8 and v_i = 2.0 no significant differences can be detected in this range. The results for a rotational speed of n = 12000 rpm confirm these tendencies.

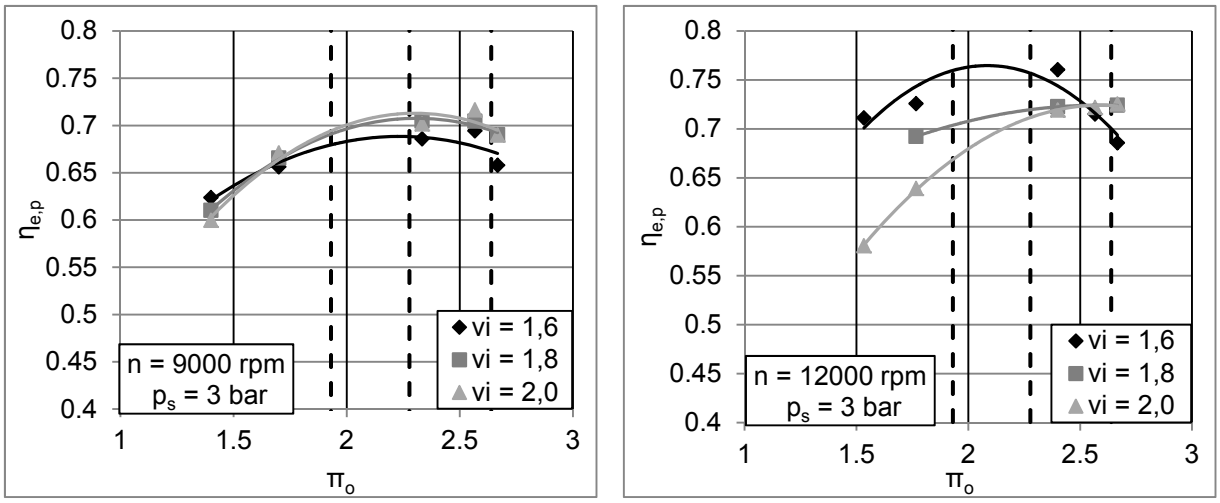

Fig. 10: Polytropic, effective efficiency as a function of the outer pressure ratio π_o for a suction pressure of p_s = 3 bar and a rotational speed of n = 9000 rpm and n = 12000 rpm

6 Comparison of simulation and experiment

6.1 Theoretical analysis of measured pressure pulsations

Pulsation excitation is calculated from the measured pressure signals in order to compare the experimental and the simulation results. Based on the assumption of plane waves, the transient pressure p̃ at an arbitrary fixed point x in the discharge piping is regarded as the superposition of an incident wave with a complex amplitude $\underline{A}$ and a reflected wave with a complex amplitude $\underline{B}$. Via the harmonic solution of the plane wave equation, the pressure as a function of time at a fixed point in space x can thus be expressed for a specific circular frequency ω with the wavenumber $k = \omega/c$ as [9]

$$\tilde{p}(t) = \underline{A}e^{j(\omega t - kx)} + \underline{B}e^{j(\omega t + kx)}. \tag{17}$$

The complex amplitude of the resultant wave at arbitrary point x is thus given by

$$\underline{p}_{mpx} = \underline{A}e^{-jkx} + \underline{B}e^{jkx} \quad . \tag{18}$$

Using eq. (18) for two of the three measuring points, a system of two equations is given for the two unknown complex amplitudes $\underline{A}$ and $\underline{B}$, which can be rearranged to obtain a solution for the amplitudes of the incident and the reflected wave in the frequency domain [10]:

$$\underline{B} = \left(\frac{\underline{p}_{mp2} - \underline{p}_{mp1} \cdot e^{jk(x_{mp1} - x_{mp2})}}{e^{jkx_{mp2}} - e^{jk(2x_{mp1} - x_{mp1})}} \right) \tag{19}$$

$$\underline{A} = \left(\frac{\underline{p}_{mp1} \cdot e^{jk(x_{mp1} + x_{mp2})} - \underline{p}_{mp2} \cdot e^{jk\,2x_{mp1}}}{e^{jkx_{mp2}} - e^{jk(2x_{mp1} - x_{mp1})}} \right) \tag{20}$$

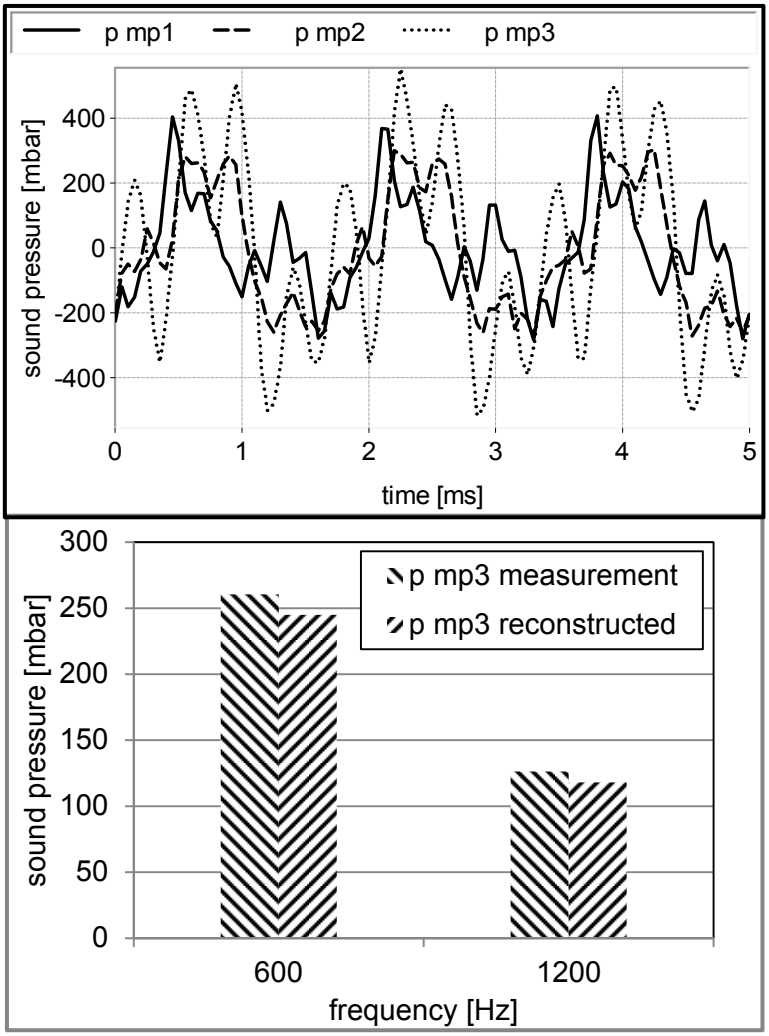

Fig. 11: Analysed and reconstructed sound pressure signal for a rotational speed of n = 9000 rpm a suction pressure of p_s = 3 bar an outer pressure ratio of π_o = 2.7 and an inner volume ratio of v_i = 1.8

The third measurement point mp_3 is used to check the result by superposing the incident and reflected wave at point x_{mp3} using eq.(18). For an exemplary operating point with a rotational speed of n = 9000 rpm and an outer pressure ratio of π_o = 2.7, the pressure signals measured at mp_1, mp_2 and mp_3 are shown in **Fig. 11**.

The pressure signals are transformed into the frequency domain and eq. (19) and (20) are applied. Complex amplitudes $\underline{A}$ and $\underline{B}$ are then superposed at mp_3 with eq. (18) and compared to the spectrum obtained from the measurement at mp_3. The significant peaks can be seen at the pocket pass frequency of f_{pp} = 600 Hz and the second harmonic. Only significant amplitudes are considered for analysis and reconstruction. Furthermore only the first two harmonics are looked at because the third harmonic is higher than the cut-off frequency of the discharge piping making the assumption of only plane waves invalid in this frequency range. For further information regarding the excitation of cross-wall modes, see [11]. Satisfactory agreement

between the measured and the reconstructed amplitudes can be recognized. The deviation amounts to 6 % for the first harmonic and 7 % for the second harmonic.

Pulsation excitation is determined by means of the sound power P_{ac}, which is the sound intensity integrated over pipe cross-sectional area A. Sound intensity for plane acoustic waves with superposed mean flow is given by [1]

$$I_{ac} = (1 + Ma)^2 \cdot \tilde{p}_{RMS} \cdot \tilde{c}_{RMS} = (1 + Ma)^2 \cdot \frac{1}{2} \hat{p} \hat{c} = (1 + Ma)^2 \cdot \frac{1}{2} \frac{\hat{p}^2}{\rho a} \quad (21)$$

where Ma is the Mach number of the mean flow, p̂ is the amplitude of the respective harmonic and ρa is the specific acoustic impedance of the mean flow. The net sound intensity I_{net} induced into the piping by the compressor amounts to the difference between the intensity of the incident wave $I_{ac,A}$ and the reflected wave $I_{ac,B}$:

$$I_{ac,net} = I_{ac,A} - I_{ac,B} \quad (22)$$

The sound power level L_W is then given by

$$L_W = 10 \cdot lg \left(\frac{P_{ac,net}}{P_0} \right) = 10 \cdot lg \left(\frac{I_{ac,net} \cdot A}{P_0} \right). \quad (23)$$

The reference power is $P_0 = 10^{-12}$ W.

6.2 Measured and simulated induced sound power level

The measured and simulated sound power level of the first and second harmonic induced by the compressor are compared in **Fig. 12** for a rotational speed of n = 9000 rpm and a suction pressure of p_s = 3 bar. For the first harmonic, the values show good agreement between simulation and experiment for v_i = 1.8 and v_i = 2.0 over a wide range of outer pressure ratios. For the highest outer pressure ratio of π_o = 2.7, the results of simulation and experiment diverge. For v_i = 1.6 good agreement between simulation and measurement can only be seen for low outer pressure ratios.

Regarding the second harmonic significant deviations can be seen between simulation and experiments throughout the range of investigated outer pressure ratios. However, the second harmonic shows a significantly lower order of magnitude than the first harmonic in both experiment and simulation.

A comparison of simulation and experimental results at n = 12000 rpm is shown in **Fig. 13**. Solely the basic harmonic of f_{pp} = 800 Hz is looked at. The trends of experimental and simulation results correspond to each other. However, significant quantitative deviations can be seen. It is assumed that deviations, especially for the inner volume ratio of v_i = 1.6, are primarily due to the proximity of the measurement points to the compressor outlet. Discharging through the pre-outlets is directed perpendicular to the direction of the mean flow (cf. fig. 3). Thus, depending on the configuration of the compressor and operating conditions, plane waves might not be fully developed at the positions of the pressure

transducers. Additionally the magnitude of the measured pulsations may be too strong to use the linear plane wave theory for weak pressure fluctuations anymore.

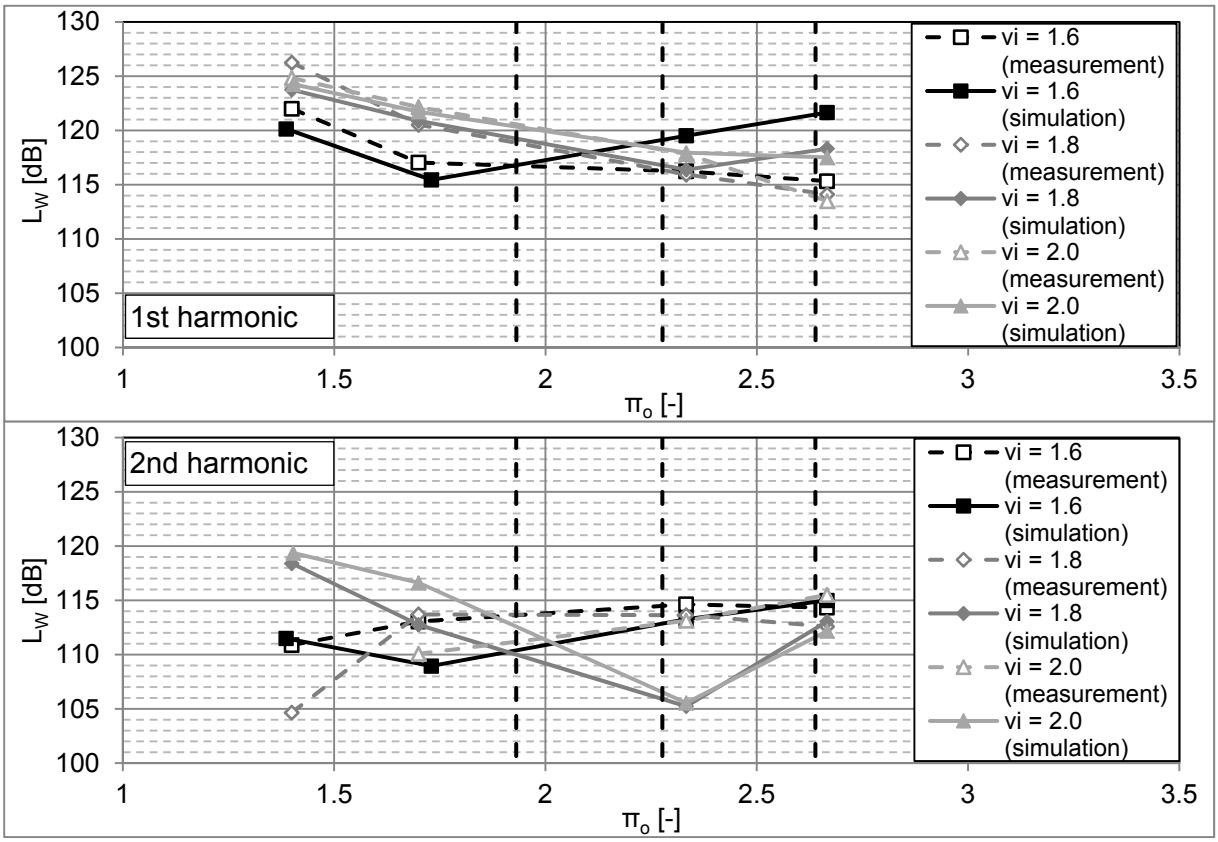

Fig. 12: Measured and simulated sound power level for the first (600 Hz) and second (1200 Hz) harmonic induced by the compressor at a rotational speed of n = 9000 rpm and a suction pressure of p_s = 3 bar

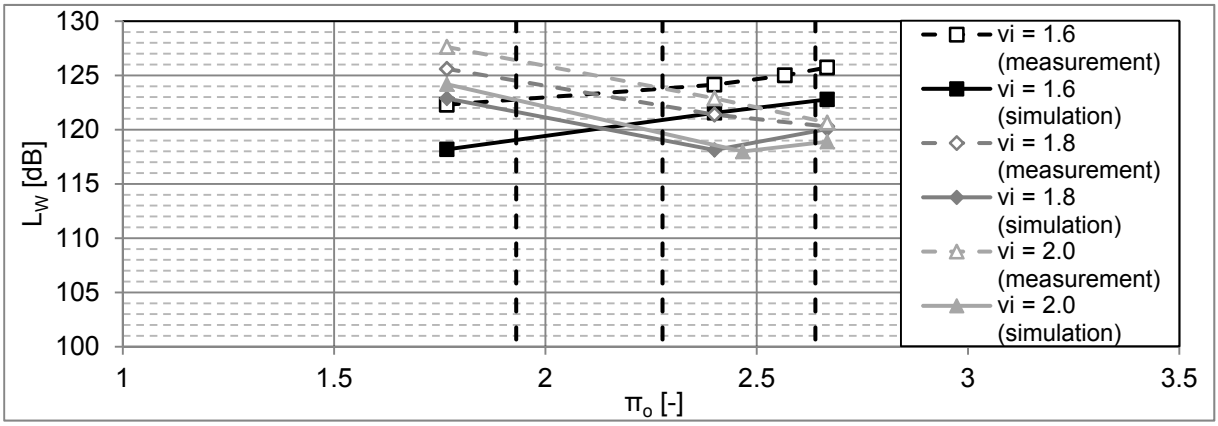

Fig. 13: Measured and simulated sound power level for the first harmonic (800 Hz) induced by the compressor at a rotational speed of n = 12000 rpm and a suction pressure of p_s = 3 bar.

7. Conclusion

A one-dimensional model of a screw compressor with variable inner volume ratio - realised by means of pre-outlet ducts - is presented. The influence of these ducts acting as dead

spaces in a closed state is presented by means of simulated pressure curves. It is shown that these additional volumes have a damping influence regarding pulsation excitation; however, power consumption is increased. Furthermore, a significant reduction in pulsation excitation by adapting the inner volume ratio to the outer pressure ratio is shown in the simulation results and experimentally proved. Potential for the reduction of power consumption is also shown.

A comparison of simulations and experimental results is carried out by calculating the induced pulsation excitation from measured pressure signals in the discharge piping. Good qualitative agreement between simulations and measurement is obtained. Depending on the operating conditions, the results also correspond quantitatively. Deviations are assumed to be primarily due to not fully developed plane waves at the position of the pressure transducers and the applied linear plane wave theory for weak pressure pulsations. In addition to further adaptions and validations of the presented model, further investigations will be carried out regarding the influence of the position of pressure transducers for the measurement of pulsation excitation by a screw compressor.

References

[1] Nickel, A.: “Entstehung von Geräuschen an trockenlaufenden Schraubenverdichtern und Möglichkeiten ihrer Reduzierung“, Fortschr.-Ber. VDI, Reihe 7, Nr. 158, VDI-Verlag, Düsseldorf, 1989

[2] Mujic, E.; Kovacevic, A.; Stosic, N.; Smith, I.K.: „Noise prediction in screw compressors“, Int. Conf. on Compressors and their Systems, 2005, p.447-454

[3] Mujic, E.; Kovacevic, A.; Stosic, N.; Smith, I.K.: “Noise generation and suppression in twin-screw compressors”, Proceedings of the Institution of Mechanical Engineers, Part E, Vol. 225 (2011) No. 2, p.127-148

[4] Große-Kracht, R.: “Schraubenverdichter für Anwendungen in Flüssigkeitskühlsätzen und Wärmepumpen“, Die Kälte- und Klimatechnik, Vol. 45 (2009), No. 5, p.33-36

[5] Hendriks, M.: „Neuer Kompakt-Schraubenverdichter mit dualer Leistungsregelung", DKV-Tagungsbericht 1999, No.1, p. 276-289

[6] Linkamp, A., Brümmer, A., “Calculation of discharge pressure pulsations of a screw compressor using the one-dimensional method of characteristics”, Proceedings of the International Conference on Compressors and their Systems, Vol. 8 (2013), p.197-207

[7] Schweinfurter, F.: “Beitrag zur rechnerischen Bestimmung von Druckschwingungen in Rohrleitungssystemen bei Erregung durch ein- und mehrzylindrige oszillierende Verdrängerpumpen”, Diss., Universität Erlangen-Nürnberg, 1988

[8] Stosic, N., Hanjalic, K.: “Contribution towards modelling of two-stage reciprocating compressors”, International Journal of mechanical Science, Vol. 19, (1977), p.439-445

[9] Zaytsev, D.: “Untersuchung von Schwingungen im Druckrohr eines ölüberfluteten Schraubenverdichters“; VDI-Berichte Nr. 1932, 2006, p. 69-81

[10] Poysat, P.; Liegeois, O.: “Measurement of gas pulsation in the discharge line of a compressor for HVAC: Method to calculate the progressive acoustic wave from the compressor and the reflected wave from the installation”; International Compressor Engineering Conference at Purdue 2006, Paper 1752

[11] Price, S.M.; Smith, D.R.: “Sources and remedies of high frequency piping vibration and noise”, Proceedings of the 28th Turbomachinery Symposium”, Vol. 28 (1999), p. 189-212